SciEn

Proceedings of 8th International Conference on Mechanical Engineering and Renewable Energy 2025
10-12 December, 2025, Chattogram, BANGLADESH

SciEn Conference Series: Engineering Vol. 4, 2026, pp 301-306 https://doi.org/10.38032/scse.2026.4.141

Design and Construction of Boiling Heat Transfer Apparatus

Mohammad Rahat Hosen, Paban Barua Nishan , Pritom Barua Shuvo, and Bodius Salam*

Department of Mechanical Engineering, Chittagong University of Engineering & Technology, Chattogram-4349, Bangladesh

ABSTRACT

Boiling heat transfer is a fundamental mechanism in thermal systems, widely applied in power generation and chemical processing. This work presents the design, development, and evaluation of a laboratory-scale apparatus to examine boiling heat transfer under controlled conditions. The setup consists of a heated metal plate submerged in water, equipped with thermocouples to record both wall and fluid saturation temperatures. A circulation unit was incorporated to maintain steady operating conditions. Experiments were performed by varying the wall superheat to capture different boiling regimes. Heat transfer coefficients (h) and heat fluxes were determined through three approaches: direct power input and surface area calculation, an empirical correlation, and the Rohsenow nucleate boiling model. Results showed that both h and heat flux increased with rising wall superheat, consistent with theoretical expectations. The empirical method produced h values in the range of 695 to 4.34×10^4 W/m²·°C. Although the measured heat flux followed predicted trends, slight deviations were attributed to thermal losses through the system. The study demonstrates that the apparatus can reliably capture boiling behavior, while also highlighting design constraints. Enhancing insulation and scaling the system could further improve accuracy and extend applicability to industrial conditions.

Keywords: Boiling Heat Transfer, Nucleate Boiling, Heat Transfer Coefficient, Thermal Management.

1. Introduction

Boiling delivers exceptionally high heat-transfer rates via liquid–vapor phase change and is fundamental to power generation, refrigeration, and chemical processing. Microchannels (μm–sub-mm scale) feature large specific surface areas and low thermal inertia, enabling efficient heat/mass transfer via extensive fluid–wall interfaces and rapid thermal responses. The concept of microchannel heat exchangers was initially introduced by Pease and Tuckerman [1]. Since then, an extensive body of research has comprehensively explored various aspects of heat transfer in microchannels, including single-phase [2] and phase change heat transfer mechanisms [3], heat transfer enhancement techniques [4], [5], and the development of microchannel heat exchange equipment [6]. Specifically, studies on single-phase convective heat transfer in microchannels have been primarily focused on optimizing geometric channel configurations and surface microtopography's, as well as leveraging work (pumping power) to achieve augmented heat transfer coefficients while mitigating the concomitant hydrodynamic penalties. The underlying heat transfer enhancement mechanisms involve both the induction of hydrodynamic perturbations in the core flow region and the manipulation of thermal boundary layer development in the near-wall vicinity [7].

The choice of heating-surface material and working fluid is critical. High-conductivity metals (e.g. copper or copper alloys) are commonly used for heater blocks and tubes [8], as they minimize thermal gradients and allow many embedded sensors. In flow-boiling annular experiments, inner tubes are often copper with custom inner fins; outer channels may be borosilicate glass or acrylic for visibility [9].More importantly, Experimental boiling heat transfer studies require carefully designed apparatus to control and measure heating, fluid, and observational parameters. Recent works describe multi-component systems comprising a power supply/control, heating element, boiling chamber, and data acquisition. For example, Xu *et al.* outline an apparatus with four subsystems (power control, solution system, data acquisition, and a heated copper column) [10], while Huang *et al.* designed a pool-boiling test rig that yielded both heat transfer coefficient (HTC) and critical heat flux (CHF) data on a pure copper surface [11]. In a high-resolution study, Fuentes *et al.* employed a double-walled boiling bath: deionized water in an inner Pyrex cell and temperature-controlled oil in an outer jacket, with embedded thermocouples and insulation to maintain uniform saturation [12]. The heating element and its materials are critical design aspects. Copper is widely used due to its high thermal conductivity. For instance, Hohl *et al.* used a horizontal copper heater of 18.2 mm diameter and 5 mm thickness, instrumented with sheathed thermocouples for wall-temperature measurement [13]. Kaneko *et al.* employed an upward-facing copper cylinder (30 mm diameter) as the heater block, with built-in heater cartridges and fins to control nucleation sites [14]. In a microchannel flow-boiling module, Qu and Mudawar cast a copper microchannel heat sink and drilled it to house twelve cartridge heaters (powered via a variable-voltage regulator) beneath the surface [15]. Surface engineering of the heating element is frequently employed to enhance boiling performance. Micro/nanostructuring and coatings are common treatments. Lin *et al.* fabricated a micro-nano roughened copper surface by sandblasting and alkali oxidation, demonstrating that such hierarchical roughness can boost CHF by ~56% and HTC by ~218% compared to a plain surface [16] New apparatus

*Corresponding Author Email Address: pritombarua75@gmail.com

designs are often validated by reproducing known boiling curves or benchmark correlations, and by comparing measured local and average HTC values with published results. For example, Xu *et al.* constructed a sophisticated microchannel test section and reported heat transfer enhancements consistent with theory [17] , while Wang *et al.* demonstrated quench-curve behavior in agreement with classic Leidenfrost-point predictions [18]. This work presents a compact laboratory-scale pool-boiling apparatus for direct measurement of wall and saturation temperatures and systematic evaluation of heat flux and heat transfer coefficients.

2. Method and Material

2.1 Apparatus Design

The boiling test rig was based on a vertical pool-boiling configurations shown in Fig. 1. A transparent cylindrical glass container served as the boiling chamber and was mounted on an insulating base block; the assembly was sealed with removable upper and lower lid plates to contain the fluid and direct vapor flow. A stainless-steel heating rod (10 mm diameter, 220 mm length) was installed vertically through the base so that its flat end formed the heated surface at the bottom of the fluid pool. This heater was powered by a controllable 1.5 kW electrical supply, enabling precise adjustment of heat input via a configurable heating block. Thermocouples were affixed directly to the heater's surface and at the fluid level (within the boiling zone) to record the heater surface temperature (T_s) and the fluid saturation temperature (T_{sat}). A calibrated pressure gauge was connected to the chamber to monitor the internal saturation pressure (P_{sat}) during boiling. All components were arranged on a rigid frame with appropriate electrical insulation and mounting to ensure stable positioning and safety.

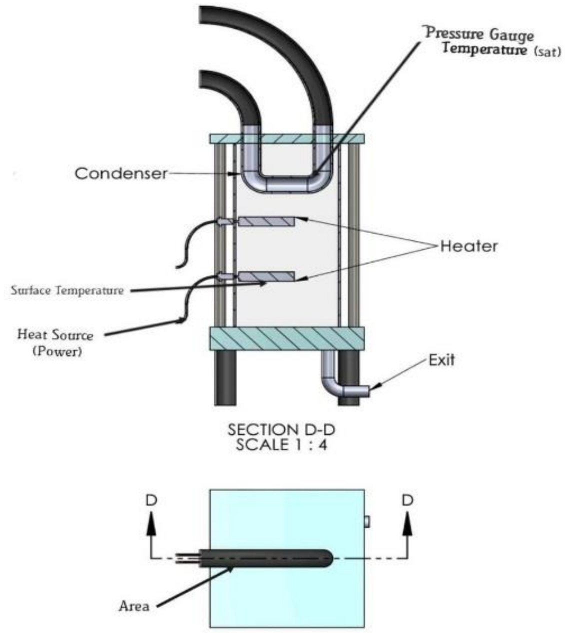

Fig. 1 Schematic representation of full design setup.

2.2 Materials Used

2.2.1 Container

A cylindrical glass vessel (type: transparent borosilicate glass), dimensions ~200 mm height × 100 mm diameter (specified in design drawings), for visual access to the boiling process. The vessel was equipped with a matching glass lid containing ports for sensor insertions.

2.2.2 Insulation Base

A thermally insulating block (e.g. ceramic or high-temperature polymer) beneath the heater to minimize heat loss to the surroundings.

2.2.3 Heating Element

Stainless steel (SS 304) immersion heater rod, 10 mm diameter by 220 mm long, chosen for corrosion resistance and high thermal conductivity. The rod was powered by a laboratory variac/DC supply capable of up to 1.5 kW output. A nickel-chrome coil surrounded by the rod (if used) was electrically connected in series for uniform heating. The heater rod is SS304 stainless steel, chosen for excellent corrosion resistance in water, mechanical strength, and adequate thermal conductivity (~16 W/m·K). Although copper (~401 W/m·K) yields higher conductivity, stainless steel is more chemically stable in aqueous boiling and easier to machine to a smooth finish. The machined rod surface has a typical finish (roughness Ra ≈0.5 µm), providing reproducible bubble nucleation sites. Deionized water is used as the working fluid for its high purity and well-characterized properties, ensuring no ionic contamination or scale that could alter boiling behavior.

2.2.4 Thermocouples

Two K-type thermocouples (±1 °C accuracy) were used: one mounted on the heater surface (bonded with thermally conductive epoxy) and one submerged in the liquid near the boiling interface. The thermocouples were connected to a digital data logger (or multimeter) via shielded wires routed through the lid ports.

2.2.5 Pressure Gauge

A mechanical Bourdon-tube gauge (range 0–2.0 kg/cm²) with 0.01 kg/cm² resolution, calibrated against a standard manometer, monitored the saturation pressure of the boiling fluid. The gauge was mounted to a side port of the container to avoid direct exposure to boiling fluid but still measure vapor pressure.

2.2.5 Fluid

Deionized water was used as the working fluid. The initial fill level was maintained at a fixed volume (e.g. 1.5 L) to ensure a consistent pool depth above the heater.

2.2.6 Auxiliary

Electrical leads, hoses (for any condensate return or filling), and fasteners (stainless steel screws, seals) were used to assemble the apparatus. All seals and joints were checked for leaks before each run.

2.3 Flow Chart

The flow chart in Fig. 2 outlines the experimental procedure, starting from setup preparation to analyzing the heat transfer coefficient. It highlights key steps such as heating, boiling observation, data acquisition, and analysis.

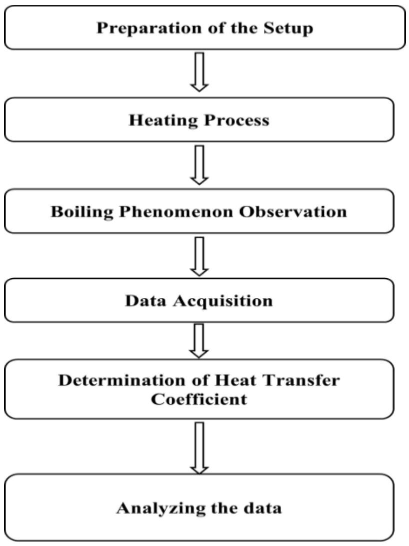

Fig. 2 Working procedure of the experiment.

2.4 Experimental Procedure

2.4.1 Assembly and Calibration

The apparatus was assembled by securing the SS heater rod into the insulated base and mounting the glass container on top. Thermocouples and the pressure gauge were installed through the lid ports: one thermocouple was attached to the heater surface and the other positioned at the fluid's saturation interface, while the pressure gauge was connected to the vapor space. Before testing, each sensor was calibrated against known references and the electrical connections to the heater were checked. The Type-K thermocouples were calibrated before use in standard ice-point and boiling-point baths, yielding an actual measurement uncertainty of ±0.5 °C. The Bourdon pressure gauge was calibrated against a U-tube manometer. Voltage and current outputs of the DC supply were measured with calibrated meters giving heater power with ~2% uncertainty. Using error propagation, we estimate the combined uncertainty in computed heat flux and HTC to be in the order of ±5%.

2.4.2 Preparation

The container was filled with a measured volume of deionized water (ensuring the immersion depth of the heater was sufficient for pool boiling but below the lid). The upper lid was then sealed, and the entire apparatus was inspected for proper insulation and grounding.

2.4.3 Heating

Electrical power was applied to the heater. The voltage/current was gradually increased (using the variac) to avoid thermal shock. The power was set to a constant 1.5 kW after initial warm-up. As the heater warmed, nucleate boiling initiated once the surface temperature exceeded the saturation point of water.

2.4.4 Data Acquisition

Once a steady boiling regime was reached (surface temperature ~105 °C with corresponding saturation around 100 °C), data collection began. Surface temperature (T_s), saturation temperature (T_{sat}), and saturation pressure (P_{sat}) were recorded at one-minute intervals for up to 10 minutes or until the system reached a thermal steady state. During each interval, the temperatures were read from the thermocouples, and the pressure was read from the calibrated gauge. The data were logged manually and/or via a computer data-acquisition system.

The experiment was repeated at least three times to ensure consistency. Between runs, the heater was turned off and the system was allowed to cool too ambient. Minor adjustments were made as needed to maintain repeatability. To minimize ambient heat loss, the boiling chamber was surrounded by foam insulation, and the glass vessel was sealed with fitted lids. The base block is an insulating ceramic to reduce conduction. The electrical power supply was operated in constant-voltage mode; we monitored voltage/current to ensure power stability (<1% variation). Steady state was defined by observing heater wall temperature and saturation pressure holding constant (±0.5°C and ±0.02 kg/cm²) for at least 3–5 minutes. Only after this criterion were data recorded.

2.5 Data Collection and Analysis Technique

2.5.1 Surface area of the heater

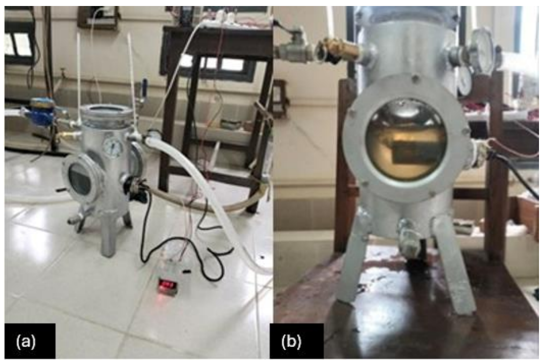

Fig. 3 (a) Boiling heat transfer apparatus; (b) Experimental setup.

The heat-transfer calculations begin with Eq. (1) the projected heating surface area A of the cylindrical heater, taken as the lateral area of the cylinder in contact with the liquid:

$$A = \pi D L \tag{1}$$

where D is the heater diameter and L is the heater active length. This is a direct geometric identity used to convert applied electrical power into an areal heat flux; identical formulations are standard in heat-transfer practice [19].

2.5.2 Heat flux

Net areal heat flux q″ is computed by Eq. (2) from the input electrical power P and the heater surface area A:

$$q'' = \frac{P}{A} \tag{2}$$

This algebraic definition (power per unit area) is the standard experimental estimate when Joule/electric power to the heater is the controlled energy input and heat losses are corrected or quantified separately. Textbooks and simulation packages use the identical expression as the starting point for flux-based analysis [20].

2.5.3 Heat-transfer coefficient

The apparent heat-transfer coefficient h (often called the boiling/film coefficient in boiling studies) is obtained by Eq. (3) from the local heat flus and the driving temperature difference

$$h = \frac{q''}{A} \quad \text{and} \quad \Delta T = T_s - T_{sat} \qquad (3)$$

This Newton-like formulation (relating flux to temperature difference) is a conventional reduction used to compare experimental results with convective/boiling correlations and to present results in units of $W\cdot m^{-2}\cdot K^{-1}$ (or $W\cdot m^{-2}\cdot {}^{\circ}C^{-1}$). See standard heat-transfer texts for this definition and for its use as a data-reduction step [20].

2.5.4 Empirical power-law relation used in the apparatus

The work also applies to a power-law empirical estimator for h of the form given by Eq. (4).

$$h = 5.56(\Delta T)^3 \qquad (4)$$

Equation (4) is an empirical power-law fit specific to our heater geometry and ΔT range. The coefficient 5.56 and exponent 3 were obtained by regression of preliminary boiling data for this setup. This correlation is not a universal law, but serves as a convenient 'empirical relation' for comparison [21].

This relation is an empirical, power-law expression reported and used directly in the apparatus data-reduction because the coefficient and exponent are not a universal physical law but an empirical fit valid for a given heater geometry, surface condition and flux range, this specific numerical form must be presented as an experimentally derived correlation in any journal submission and supported either by (a) the original source that tabulated it or (b) the thesis' own fit procedure and scatter analysis. In the present case the coefficient/exponent pair appears in the thesis and should be explicitly described as such in the Methods [21].

2.5.5 Rohsenow pool-boiling correlation (theoretical/empirical hybrid)

To compare measured fluxes with classical nucleate-boiling models the Rohsenow correlation was applied. The Rohsenow form relates q″ to the wall superheat and a surface–fluid factor Csf; a commonly used dimensional representation is

$$q'' = \mu_l h_{fg} \left[\frac{C_{pl}\,\Delta T}{C_{sf}\, h_{fg}\, pr^n}\right]^3 \left(\frac{g(\rho_l - \rho_v)}{g_0\, \sigma}\right)^{\frac{1}{2}} \quad (5)$$

where symbols denote standard thermophysical properties: μ_ℓ (liquid dynamic viscosity), h_{fg} (latent heat of vaporization), $c_{p\ell}$(liquid specific heat), Pr (Prandtl number), g(gravitational acceleration), ρ_ℓ ,ρv (liquid and vapour densities) and σ (surface tension). The dimensionless surface factor C_{sf} accounts for the liquid–surface combination and is found in Rohsenow's tabulations or by regression of experimental data.

3. Result and Discussion

The experimental results obtained from the system and interpreted using both empirical methods and theoretical models, including the Rohsenow correlation. The relationship between temperature difference (ΔT), heat flux (q″), and the heat transfer coefficient (h) is examined to understand the effectiveness and limitations of the apparatus in promoting nucleate boiling.

Below Table 1 shows heat transfer coefficient from direct measurement, simplified model and Rohsenow correlation.

Heat losses (conduction through the base and radiation/convection to air) were estimated by a calibration test without fluid contact. We found that at high input (~1.5 kW), conduction through the base accounted for ~8–10% of power. All reported heat fluxes were corrected by subtracting the measured loss power.

Table 1 Heat transfer coefficient value

Surface Temperature, T_s (°C)	Saturation Temperature, T_{sat} (°C)	Power based, h = P / A(ΔT) ($W/m^2\cdot{}^{\circ}C$)	Emperical relation Based, $h = 5.56(\Delta T)^3$ ($W/m^2\cdot{}^{\circ}C$)	q" (W/m^2) (Rohsenow)	Rohsenow Correlation Based, h = q" /(ΔT) ($W/m^2\cdot{}^{\circ}C$)
105	100	43405.89	695	11990.74	2398.15
107	101	36171.58	1200.96	20719.99	3453.33
110	103	31004.21	1907.08	32902.59	4700.37
112	104	27288.68	2846.72	49114.87	6139.26
114	106	27288.68	2846.72	49114.07	6139.26
116	108	27288.68	2846.72	49114.07	6139.26
118	109	24114.38	4053.24	69929.99	7769.99
120	110	21702.95	5501	95925.92	9592.59
122	111	19729.95	7400.36	127677.40	11607.04
124	112	18085.79	9607.68	165759.99	13813.33

3.1 Graphical Representation

In Fig. 4 compares the heat transfer coefficients between the power-based and empirical relation-based methods, with ΔT (temperature difference) on the x-axis.

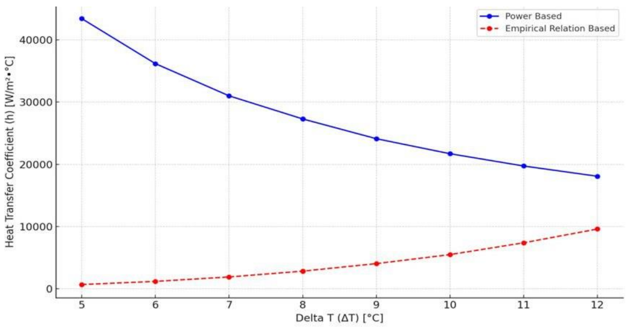

Fig. 4 Heat Transfer coefficient comparison (power-based vs emperical relation based)

Fig. 4 compares heat transfer coefficients obtained from the power-based and empirical methods as a function of ΔT. The power-based method shows a decrease in HTC with increasing ΔT, which is counterintuitive, while the empirical method shows a consistent increase, matching expected boiling behavior. This apparent decrease arises because heat losses through the base and walls were not subtracted in the power-based calculation; as ΔT increases, a larger fraction of input power is lost to the surroundings. When heat losses are accounted for, both the empirical and Rohsenow-based HTC increase with ΔT as expected. Similar trends have been reported in the literature, where proper insulation restores the correct boiling curve behavior. In Fig. 5 the power-based method showed a sharp decline in heat transfer coefficient as ΔT increased, indicating a high sensitivity to temperature differences.

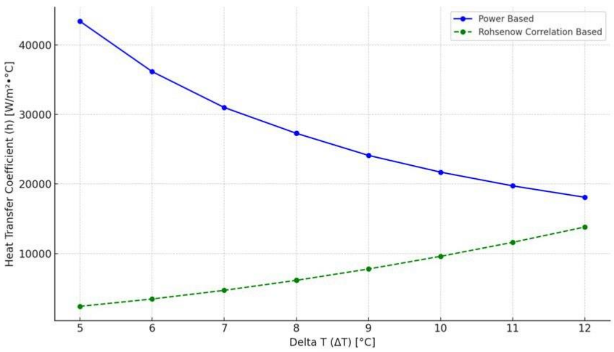

Figure 5: Heat transfer coefficient comparison (power based bs Rohsenow correlation based)

The graph compares the heat transfer coefficients between the power-based method and the Rohsenow correlation-based method, with ΔT (temperature difference) on the x-axis. In contrast, the Rohsenow correlation-based method displayed a gradual increase in heat transfer coefficient with ΔT, reflecting more typical physical behavior where heat transfer improves with larger temperature gradients.

Fig 6 the power-based method showed a rapid decline in heat transfer coefficient as ΔT increased, indicating a high sensitivity to temperature differences.

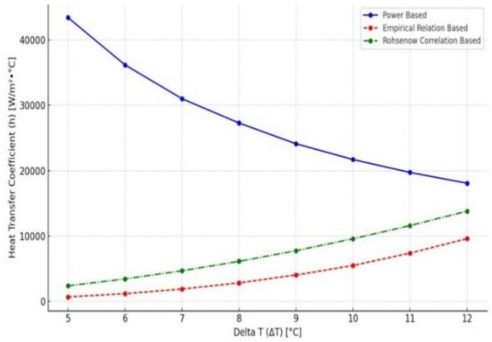

Fig. 6 Heat transfer coefficient comparison (power based, emperical relation based and Rohsenow correlation based)

The graph compared the heat transfer coefficients from three different methods: power-based, empirical relation-based, and Rohsenow correlation-based, with ΔT as the x-axis. In In contrast, the empirical relation-based method exhibited a steady increase in heat transfer coefficient with ΔT, aligning more closely with typical physical behavior, where heat transfer improves with larger temperature differences. The Rohsenow correlation-based method displayed a gradual increase similar to the empirical method, but with slightly higher values, suggesting it might have been more accurate at predicting heat transfer in systems with larger temperature gradients. Heat loss was likely a factor contributing to the variations observed in the power-based method, as the decreasing temperature difference reduced the heat transfer efficiency.

The boiling heat transfer apparatus was designed and tested to evaluate heat transfer coefficient and heat flux during boiling. Results showed that both parameters increased with surface temperature, consistent with theoretical expectations. The power-based method yielded higher HTC values than empirical correlations. Measured HTC values (7×10^2–4.3×10^4 W/m²·°C) agreed with reported pool boiling data. Differences between theory and experiment were mainly due to unaccounted heat losses, though the apparatus effectively demonstrated boiling heat transfer behavior.

4. Conclusions

Boiling heat transfer apparatuses play a critical role in industries that rely on high-efficiency heat transfer processes, such as power generation, chemical processing, and food production. Efficient heat transfer during boiling is essential for optimizing energy use, reducing costs, and improving process efficiency. The design of this boiling heat transfer apparatus offers a simple yet effective solution for understanding heat dissipation and transfer in such processes. The experimental results highlight both the strengths and limitations of the current design, such as its capacity for heat transfer, sensitivity to different calculation methods, and the impact of heat loss through the system. The findings suggest that improvements in insulation and scaling up the apparatus can significantly enhance performance, making it more suitable for industrial applications.

5.References

[1] Tuckerman, D.B. and Pease, R.F.W., 2005. High-performance heat sinking for VLSI. *IEEE Electron device letters*, *2*(5), pp.126-129.

[2] Han, Q., Liu, Z., Zhang, C. and Li, W., 2024. Enhanced single-phase and flow boiling heat transfer performance in saw-tooth copper

microchannels with high L/Dh ratio. *Applied Thermal Engineering*, *236*, p.121478. Li, Y., Zhu, C., Li, X. and Yang, B., 2025. A review of non-uniform load distribution and solutions in data centers: micro-scale liquid cooling and large-scale air cooling. *Energies*, *18*(1), p.149.

[3] Liu, X., Yang, J., Zou, Q., Hu, Y., Li, P., Tan, L., Miljkovic, N. and Yang, R., 2025. Enhancing Liquid–Vapor Phase-Change Heat Transfer with Micro/Nano-Structured Surfaces. *ACS nano*, *19*(10), pp.9513-9589.

[4] Jiang, H., Zhao, X. and Zhang, M., 2024. Boiling Heat Transfer Characteristics of Noah-2100A and HFE-649 in Pin-Fin Microchannel Heat Sink. *Energies*, *17*(24), p.6216.

[5] Yih, J. and Wang, H., 2020. Experimental characterization of thermal-hydraulic performance of a microchannel heat exchanger for waste heat recovery. *Energy Conversion and Management*, *204*, p.112309.

[6] M. Asadi, G. Xie, and B. Sunden, "A review of heat transfer and pressure drop characteristics of single and two-phase microchannels," *Int J Heat Mass Transf*, vol. 79, pp. 34–53, 2014, doi: 10.1016/j.ijheatmasstransfer.2014.07.090.

[7] Basavaraj, A.K., Zajec, B. and Matkovič, M., 2018, September. Accurate measurements of the Local Heat Transfer coefficients along the dedicated test section. In *Proceedings of NENE 2018, 27th International Conference Nuclear Energy for New Europe*.

[8] Vargas, B.A.d.F., Constantino, M. & Kanizawa, F.T., 2021. *Development of a test section for determination of local heat transfer coefficient during in-tube flow*. In: *Proceedings of COBEM 2021*.

[9] Kumar, G. and Madanan, U., 2023. Factors influencing heat transfer mechanism in nucleate pool boiling: A comprehensive review with state of the art and future prospects. *Advances in Heat Transfer, 56*, pp.435-582.

[10] Xu, C., Ren, J., Qian, Z. and Zhao, L., 2024. Investigation of Heat Transfer Performance in Deionized Water–Ethylene Glycol Binary Mixtures during Nucleate Pool Boiling. *Processes*, *12*(2), p.368.

[11] Zhang, L., Wang, C., Su, G., Kossolapov, A., Matana Aguiar, G., Seong, J.H., Chavagnat, F., Phillips, B., Rahman, M.M. and Bucci, M., 2023. A unifying criterion of the boiling crisis. *Nature communications*, *14*(1), p.2321.

[12] Hohl, R., Blum, J., Buchholz, M., Lüttich, T., Auracher, H. and Marquardt, W., 2001. Model-based experimental analysis of pool boiling heat transfer with controlled wall temperature transients. International journal of heat and mass transfer, 44(12), pp.2225-2238.

[13] Suroto, B.J., Tashiro, M., Hirabayashi, S., Hidaka, S., Kohno, M. and Takata, Y., 2013. Effects of hydrophobic-spot periphery and subcooling on nucleate pool boiling from a mixed-wettability surface. *Journal of Thermal Science and Technology*, *8*(1), pp.294-308.

[14] Al-Waaly, A., 2024. Numerical Investigation of the Impact of Subcooling Inlet on Water Flow Boiling Heat Transfer Through a Microchannel. Wasit Journal of Engineering Sciences, 12(2), pp.92-109.

[15] Rivera, W. and Best, R., 1999. Boiling heat transfer coefficients inside a vertical smooth tube for water/ammonia and ammonia lithium nitrate mixtures. *International Journal of Heat and Mass Transfer*, *42*(5), pp.905-921.

[16] Xu, Z., Zhang, W., Zhang, Q., Zhai, X., Yang, X., Deng, Y. and Wang, X., 2025. Experimental Study on Flow Boiling Heat Transfer Characteristics in Top-Connected Microchannels with a Ni/Ag Micro/Nano Composite Structure. *Energies*, *18*(7), p.1756.

[17] Kruse, C., Anderson, T., Wilson, C., Zuhlke, C., Alexander, D., Gogos, G. and Ndao, S., 2013. Extraordinary shifts of the Leidenfrost temperature from multiscale micro/nanostructured surfaces. *Langmuir*, *29*(31), pp.9798-9806.

[18] Heat Flux, *n.d.* Available at: http://www.abcde.com/fghij/klmn/op123 (Date of access: 12 October 2025).

[19] Price, M.L., Matthews, M.A. & Papathansiou, T., *n.d. Heat transfer analysis in solids*. University of South Carolina, ECHE 460 Chemical Engineering Laboratory I. Available at: https://cse.sc.edu/~gatzke/460/F-Heat%20Conduction.pdf (Date of access: 10 October 2025).

[20] Heat Transfer Coefficients - Expert Guide - Volupe, *n.d.* Available at: https://volupe.com/support/empiricalcorrelations-for-convective-heat-transfercoefficients/ (Accessed: 28 October 2025).

[21] Sarkar, D., Savory, E. and DeGroot, C., 2023. Thermodynamic modeling of thermosyphons and heat pipes. *Physics of Fluids*, *35*(12).